J Mol Model (2013) 19:5515–5521
DOI 10.1007/s00894-013-2047-x

ORIGINAL PAPER

A density functional theory study on oxygen reduction reaction on nitrogen-doped graphene

Jing Zhang · Zhijian Wang · Zhenping Zhu

Received: 19 August 2013 / Accepted: 21 October 2013 / Published online: 17 November 2013

Abstract Nitrogen (N)-doped carbons reportedly exhibit good electrocatalytic activity for the oxygen reduction reaction (ORR) of fuel cells. This work provides theoretical insights into the ORR mechanism of N-doped graphene by using density functional theory calculations. All possible reaction pathways were investigated, and the transition state of each elementary step was identified. The results showed that OOH reduction was easier than O–OH breaking. OOH reduction followed a direct Eley–Rideal mechanism (the OOH species was in gas phase, but H was chemisorbed on the surface) with a significantly low reaction barrier of 0.09 eV. Pathways for both four-electron and two-electron reductions were possible. The rate-determining step of the two-electron pathway was the reduction of O_2 (formation of OOH), whereas that of the four-electron pathway was the reduction of OH into H_2O. After comparing the barriers of the rate-determining steps of the two pathways, we found that the two-electron pathway was more energetically favored than the four-electron pathway.

Keywords Density functional theory · Nitrogen-doped carbon · Oxygen reduction reaction · Reaction mechanism

Introduction

Fuel cells are an efficient power generation source with high efficiency and low emission. They are expected to have a significant contribution in the efficient use of energy in the near future [1, 2]. In this system, the cathodic half-reaction or the reduction of oxygen into water limits the performance of fuel cells because of its multi-electron reaction character and low reaction rate [3]. The development of efficient catalysts for oxygen reduction reaction (ORR) is crucial in the practical applications of fuel cells. Platinum (Pt)-based materials are the most widely used catalysts for ORR [4, 5]. However, the commercial application of fuel cells is limited by the low durability, scarcity, and high cost of Pt [6].

In the past few decades, intensive efforts have been performed to reduce Pt usage or replace it completely. Researchers [7–20] have recently found that nitrogen (N)-doped carbons, including N-doped carbon nanotubes, graphene sheets, and graphitic arrays, exhibit excellent electrocatalytic performance. These materials have become promising candidates to replace Pt-based catalysts. However, the detailed ORR mechanisms of these N-doped carbons remain unclear, and several issues remain unaddressed. First, whether or not the doped N atoms really improve ORR is still debatable because the employed N-doped carbon materials are usually synthesized using metal catalysts whose residues often enhance ORR activity [17]. Zhang et al. [21] reported that N-doped graphene (without Fe) exhibits low ORR activity because of the absence of Fe ions. Second, X-ray photoelectron spectroscopy results showed that three types of N species, namely, graphite-like, pyridine (or pyridinium)-like, and pyrrole-like N atoms, may simultaneously exist in N-doped carbons. However, previous studies have not made a consensus on which types of N atoms, i.e., graphitic, pyridinic, pyrrolic, or two of three or even all types, are active structures. Several reports have suggested that graphite-like N [9, 11, 18, 19] exhibits high ORR catalytic activity, whereas others have concluded that both graphite-like and pyridine-like N species can activate oxygen [22, 23]. Moreover, others have indicated that pyridine-like N cannot induce ORR activity [12] and even have a tendency to suppress ORR activity [12, 24]. Experimental techniques are not effective tools in identifying active

J. Zhang · Z. Wang · Z. Zhu (✉)
State Key Laboratory of Coal Conversion, Institute of Coal Chemistry, Chinese Academy of Sciences, Taiyuan, Shanxi 030001, China
e-mail: mhs913@163.com

J. Zhang
School of Chemical and Biological Engineering, Taiyuan University of Science and Technology, Taiyuan, Shanxi 030021, China

J. Zhang
University of Chinese Academy of Sciences, Beijing 100039, China

sites because the effects of edge N and pyridine-like N are difficult to distinguish [25]. Gaussian [26] simulation was used to study pyridine-like and pyrrole-like N-containing graphene sheets. The results showed that these two N species have ORR activities. Third, whether or not the ORR on N-doped carbons undergoes a four-electron or two-electron pathway remains unknown. Ikeda et al. [27] proposed that the four-electron ORR pathway could be achieved by doping graphite-like N. However, other scholars [28–30] have suggested that ORR predominantly occurs through the two-electron pathway with H_2O_2 as the final product. Okamoto et al. [31] found a pathway to 4e reduction on the structure of graphite-like N. However, the occurrence of second reduction before O–OH breaking suggests that a pathway to 2e reduction exists. Luo et al. [32] synthesized a pyridinic N-doped graphene. In this case, the ORR was a two-electron pathway. However, Qu et al. [8] synthesized N-doped graphene containing pyridine-like and pyrrole-like N atoms, where oxygen was reduced via a four-electron pathway.

The ORR on N-doped carbon materials has attracted considerable attention. However, many problems still persist. Although several researchers focused on the mechanism of ORR on N-doped carbons [25, 26, 31, 33], they [25, 26, 31] only studied the reaction pathway and obtained no quantitative information of reaction kinetics, such as reaction barriers. Yu et al. [33] obtained information about reaction kinetics but only studied the four-electron ORR pathway in an alkaline solution. In the present work, we used the density function theory (DFT) method to investigate all possible ORR pathways, including four-electron and two-electron pathways. This study aims to examine the reaction mechanism, particularly the kinetics of the ORR on N-doped graphene catalysts. The catalytic active site was examined. Energy variations and reaction barriers were calculated for each fundamental step, the rate-determining step was determined, and the most feasible ORR pathway on the N-doped graphene was analyzed. In this work, only graphite-like N structure was considered because most reports suggested it has ORR activity.

Methods and models

DFT method

All calculations were performed using the Dmol^3 module in the Materials Studio program of Accelrys Inc [34, 35]. The exchange and correlation energies were calculated using the Perdew, Burke, and Ernzerhof functions (PBE) [36] with generalized gradient approximation (GGA) [37]. Double numerical plus polarization function (DNP) basis sets were employed in the calculation. Spin polarization, which has significant effects on the adsorption energies for magnetic systems [38], was included, and a 5×5×1 k-point set was used. The geometry convergence tolerance for energy change, max force, and max displacement were 0.00001 hartree, 0.002 hartree Å^{-1}, and 0.005 Å, respectively. We used the complete linear synchronous transit/quadratic synchronous transit method to search for the transition states. The reaction energy and activation barrier of each elementary step are listed in Table 1.

Model

We applied a 6×6 graphene supercell that has 72 C atoms with one doped graphite-like N atom substituting a C atom (Fig. 1). A periodic boundary condition was used. In the vertical direction, a vacuum slab was set to at least 15 Å to avoid interplanar interactions. The adsorption energy E_{ads} was defined as $E_{ads} = E_{tot} - E_{dg} - E_X$, where E_{tot} is the total energy of the doped graphene with an adsorbed X species, E_{dg} is the energy of doped graphene, and E_X is the energy of an isolated X species. The same supercell and k-point grids were used for all calculations to minimize systematic errors. The ORR at solid–liquid interfaces is rather complex because they involve solid surfaces, solvent, and substrates. Therefore, simulating such processes by using a simple model system at the solid–gaseous interface seems difficult. However, the results of these simple models facilitate a better understanding of complex systems (heterogeneous liquid-phase catalysis).

No local distortion was observed when N was doped in graphene, except for minimal changes. This result is similar to that reported by Dai et al. [39]. The C–C length of graphene was 1.42 Å after optimization. After N doping, the average length of C–N was 1.41 Å, which is in agreement with the result of Zhao et al. [40]. Furthermore, the electronegativity of N was larger than that of C, and the doped N induced charge delocalization. The result of Mulliken population analysis showed that the N atom and its neighboring C atoms showed negative and positive charges, respectively. The N atom had a negative charge of −0.458 e. Most of the compensating positive charges were distributed on the three nearest neighboring C atoms with a positive charge of 0.178 e. This result is in agreement with the result of Gong et al. [5].

Table 1 Reaction energy (E_{rea}) and activation barrier (E_{act}) of each reaction step

Reaction step	E_{rea}(eV)	E_{act}(eV)
$O_2 + H_{(ads)} \rightarrow OOH_{(ads)}$	−0.96	0.63
$OOH_{(ads)} \rightarrow O_{(ads)} + OH_{(ads)}$	0.25	1.18
$OOH_{(ads)} + H_{(ads)} \rightarrow O_{(ads)} + H_2O$	−2.99	0.55
$OOH_{(ads)} + H_{(ads)} \rightarrow 2OH_{(ads)}$	−2.91	0.72
$O_{(ads)} + H_{(ads)} \rightarrow OH_{(ads)}$	−2.21	0.54
$OH_{(ads)} + H_{(ads)} \rightarrow H_2O$	−2.23	0.82
$OOH_{(ads)} + H_{(ads)} \rightarrow OOH + H_{(ads)}$	0.16	0.23
$OOH + H_{(ads)} \rightarrow H_2O_2$	−2.21	0.09
$H_2O_2 \rightarrow 2OH_{(ads)}$	−0.48	1.39

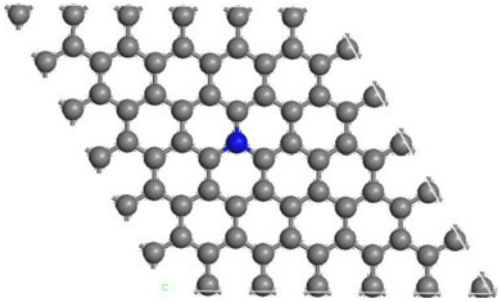

Fig. 1 Optimized structure of GNDG. The *gray* and *blue spheres* represent C and N atoms, respectively

Results and discussion

Adsorption of O_2 on N-doped graphene

The bond length of O_2 molecule in the ground state was 1.225 Å (experimental value is 1.209 Å). The O_2 molecule was initially placed at all possible adsorption sites, such as the top sites of N and C atoms, the bridge sites of N–C and C–C bonds, and the center site of the hexagonal lattice. After relaxation, O_2 was adsorbed on the graphite-like N-doped graphene (GNDG) with a small adsorption energy of −0.20 eV and a long distance of 3.20 Å from the graphene plane, which suggests that the interaction between the O_2 molecule and the surface was weak. This result is consistent with that of Dai et al. [39]. Many reports [25, 27, 28, 39] suggested that the O_2 molecule is physically adsorbed on N-doped graphene, which is different from the ORR mechanism on Pt-based materials [41–49]. O_2 is chemically adsorbed on the Pt (111) surface with an adsorption energy of −0.96 eV [43].

Chemical behavior of adsorbed oxygen

The adsorption of O_2 molecule has two possible reaction pathways, namely, dissociation or formation of the OOH species. First, we considered the dissociation of the adsorbed O_2. This dissociation reaction is expressed in Eq. (1), where the subscript (ads) represents the adsorption on the surface. This reaction was endothermic with a reaction energy (the change in the total energy between productions and reactants) of 1.20 eV, which indicates that O_2 dissociation was energetically unfavorable.

$$O_{2(ads)} \rightarrow 2O_{(ads)} \quad (1)$$

Alternatively, the $O_{2(ads)}$ molecule may seize an H atom to form an $OOH_{(ads)}$ species. The formation of $OOH_{(ads)}$ is expressed in Eq. (2). After the O_2 molecule was adsorbed on the surface, we introduced an H atom into the system. After relaxation, the O_2 molecule was activated by the presence of the adsorbed H, and the OOH species was then formed. As shown in Fig. 2, the formed OOH was adsorbed chemically on the GNDG surface, and the most favorable adsorption site was the top site of the C atom next to the doped N atom with an adsorption energy of −0.88 eV. This finding is in agreement with other theoretical results [33, 50]. After the adsorption of OOH on the C atom, the latter moved out of the surface plane and the distance between the C and O atoms of OOH was 1.49 Å, which is close to the value (1.50 Å) reported by Zhang et al. [26].

$$O_{2(ads)} + H^+ + e^- \rightarrow OOH_{(ads)} \quad (2)$$

Reaction (2) is a crucial step for the catalytic activity of N-doped carbons because the adsorption and formation of chemical bonds are necessary for the following reactions [26]. The reaction energy and activation barrier of reaction (2) were −0.96 and 0.63 eV, respectively, which indicates that the reaction was exothermic. In terms of thermodynamics and kinetics, reaction (2) was a favorable pathway for O_2. Therefore, hydrogen-mediated adsorption should be the dominant process in the reduction of O_2.

The adsorption of $OOH_{(ads)}$ has two possible reaction pathways. One is to combine with an H atom and produce H_2O_2, the other is to break the O–OH bond and form the final product, H_2O. The former is a two-electron reaction pathway, and the latter is a four-electron reaction pathway.

Two-electron pathway

The formation of H_2O_2 is expressed in Eq. (3a). After $OOH_{(ads)}$ was adsorbed on the GNDG surface, we introduced another H to the system. The H atom was placed near the O atom that was bonded to the C atom to produce H_2O_2 (Fig. 3a). The final optimized structure of H_2O_2 on the surface is shown in Fig. 3c, in which the formed H_2O_2 drifted away from the surface. The nearest distance between the molecule and surface was 3.41 Å. This work failed to identify the transition state of this step. To the best of our knowledge, no study has ever reported on the

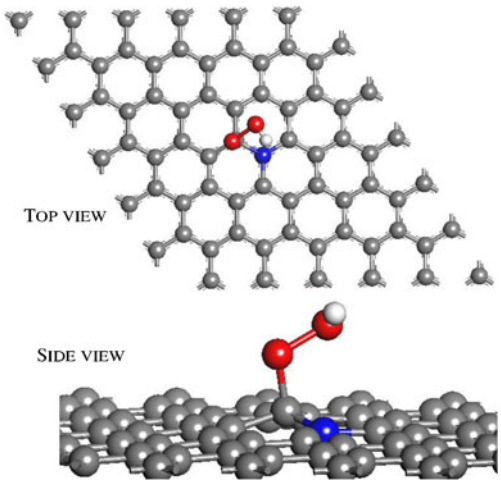

Fig. 2 Top view (**a**) and side view (**b**) of the most stable configuration of OOH on GNDG. (*gray*, *blue*, *red*, and *white spheres* represent C, N, O, and H atoms, respectively)

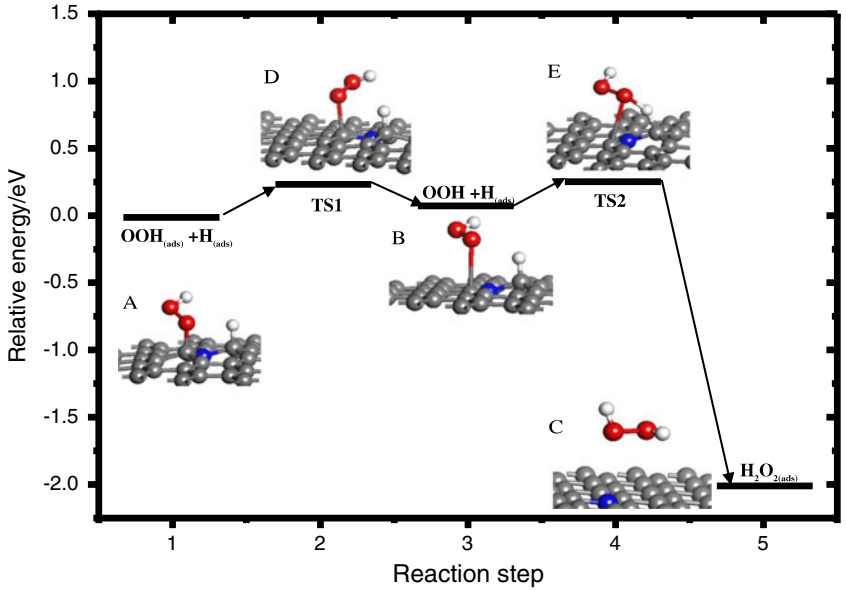

Fig. 3 Relative reaction energy and activation barrier of OOH reduction to form H_2O_2 on the surface together with optimized reactant and product structures and corresponding transition structures. **a** Adsorbed OOH and H species. **b** Stable adsorbed H and desorbed OOH. **c** Generated H_2O_2. **d** and **e** are the two corresponding transition states

reaction barrier of H_2O_2 formation on N-doped carbon materials. In fact, the calculation results show that this reaction was not an elementary step but included two steps. First, the adsorbed OOH was desorbed from the surface (Fig. 3b), the distance between the OOH to the surface increased from 1.50 Å to 2.56 Å, and the O–O bond decreased from 1.49 Å to 1.39 Å. Second, the desorbed OOH combined with the adsorbed H atom, and the O–O bond was increased to 1.47 Å. The H_2O_2 molecule was then formed, which indicates that the formation of H_2O_2 followed a direct Eley–Rideal (ER) mechanism [51] rather than a Langmuir–Hinshelwood (LH) mechanism. In the ER mechanism, molecules from the gas react with surface-chemisorbed reagents. In the LH mechanism, both reagents are chemisorbed on the surface [52, 53]. The schematic of these two reaction steps is shown in Fig. 3. As shown in the figure, OOH desorption is an endothermic process that absorbed an energy of 0.16 eV and had a desorption barrier of 0.23 eV. The structure of the transition state is shown in Fig. 3d. The reduction of OOH into H_2O_2 is an exothermic reaction that released an energy of −2.21 eV and had an active barrier of 0.09 eV, which was very low such that the H_2O_2 molecule was easily formed. Thus, the ORR is a two-electron pathway. However, if the formed H_2O_2 easily caused O–O breaking and generated two OH species, then the ORR remains as a four-electron pathway. Thus, we considered the dissociation of H_2O_2.

$$OOH_{(ads)} + H^+ + e^- \rightarrow H_2O_{2(ads)} \quad (3)$$

$$H_2O_{2\ (ads)} \rightarrow 2OH_{(ads)} \quad (4)$$

The products of H_2O_2 dissociation were two OH species, which were adsorbed on the C atoms next to the N atom. The reaction is expressed in Eq. (4). The reaction energy and active barrier of this step were −0.48 and 1.39 eV, respectively. The results show that this reaction released heat to proceed. However, the barrier value of 1.39 eV was too high to be overcome at the working condition of the fuel cell [33]. Therefore, the formed H_2O_2 was difficult to dissociate, which indicates that the ORR may be a two-electron reaction pathway on GNDG. This conclusion was consistent with the experimental and theoretical results [28–30]. Compared with the barriers of all elementary steps along the two-electron pathway, the reduction of O_2 into OOH had the highest barrier 0.63 eV, which indicates that it is the rate-determining step of the whole two-electron ORR pathway.

Four-electron pathway

The breaking of the O−OH bond is an important step because it indicates a four-electron reaction pathway [26]. The adsorbed $OOH_{(ads)}$ has three possible dissociation pathways:

$$OOH_{(ads)} \rightarrow O_{(ads)} + OH_{(ads)} \quad (5)$$

$$OOH_{(ads)} + H^+ + e^- \rightarrow H_2O_{(ads)} + O_{(ads)} \quad (6)$$

$$OOH_{(ads)} + H^+ + e^- \rightarrow 2OH_{(ads)} \quad (7)$$

Equation (5) expresses the pathway of direct dissociation of $OOH_{(ads)}$, in which the products were O and OH species. These two products were chemically adsorbed on the doped surface, and the favorable adsorption sites were the top sites of C atoms next to the N atom. As shown in Table 1, this reaction was slightly endothermic, where an energy of only 0.25 eV was absorbed. However, the barrier of this reaction was remarkably large (1.18 eV). At the working temperature of fuel

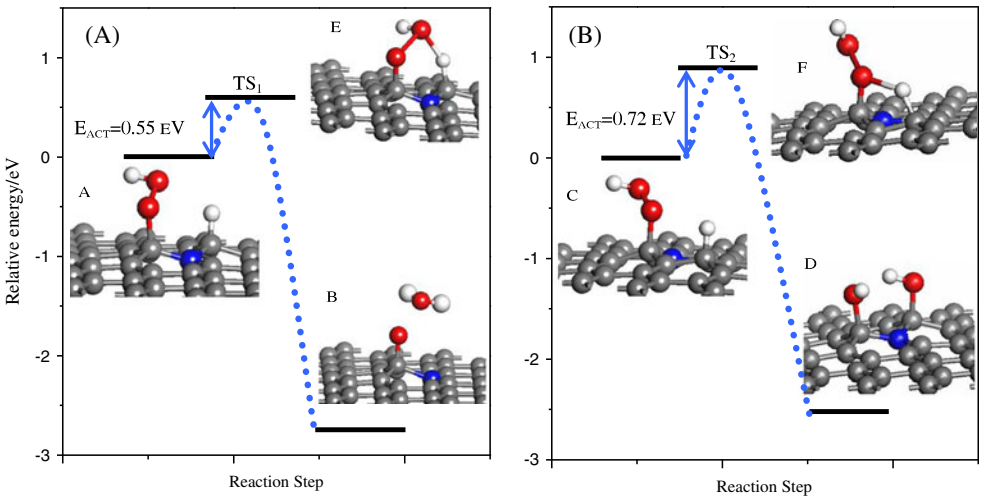

Fig. 4 Relative reaction energy and activation barrier of OOH reduction on surface together with optimized reactant and product structures and corresponding transition structures. **a** Reduction to form $O_{(ads)}$ and H_2O. **b** Reduction to form two $OH_{(ads)}$

cell (approximately 350 K), a barrier of 1.18 eV was difficult to overcome, which indicates that direct $OOH_{(ads)}$ dissociation is difficult to occur at a reasonable rate on the GNDG surface. Zhang et al. [44] found that OOH dissociation is one of the steps that kinetically limit the electrocatalytic oxygen reduction on a Pt surface.

Instead of breaking the O–OH bond directly, $OOH_{(ads)}$ can break the bond with the help of the introduced H atom. This reaction is called hydrogenation dissociation in the present work. Another H atom was then introduced into the system. This H atom may randomly move to the position near the O atom that was bonded to the H atom (Fig. 4a) or the other oxygen atom (Fig. 4c) [26]. The former reaction is expressed in Eq. (6), and the optimized structure is shown in Fig. 4b. The O atom that was initially adsorbed on the C atom remained bonded to it, whereas the OH moiety combined with the introduced H atom and generated an H_2O molecule. The formed H_2O molecule drifted away from the surface, and the nearest distance between the H_2O molecule and the surface was 3.12 Å. The distance between the two O atoms was 1.98 Å, which indicates that the O–O bond was broken.

The reaction wherein the introduced H was close to the O atom that was bonded to the C atom is expressed in Eq. (7). The optimized structure (Fig. 4d) shows that the O atom combined with the introduced H atom and was still bonded to the C atom in the form of $OH_{(ads)}$. Meanwhile, the other OH moiety drifted away and was adsorbed on another C atom next to the N atom. The distance between the two O atoms was 2.73 Å, which indicates that the O–O bond was broken.

The schematic of these two reactions is shown in Fig. 4. The reaction energies of Eqs. (6) and (7) were −2.99 and −2.91 eV, respectively, which indicate that these two reactions were strongly exothermic and therefore energetically favorable. The dissociation barriers of reactions (6) and (7) were 0.55 and 0.72 eV, respectively. The corresponding transition state structures are shown in Fig. 4e and f. The barriers of hydrogenation dissociation pathways, which are shown in reactions (6) and (7), were lower than that of direct

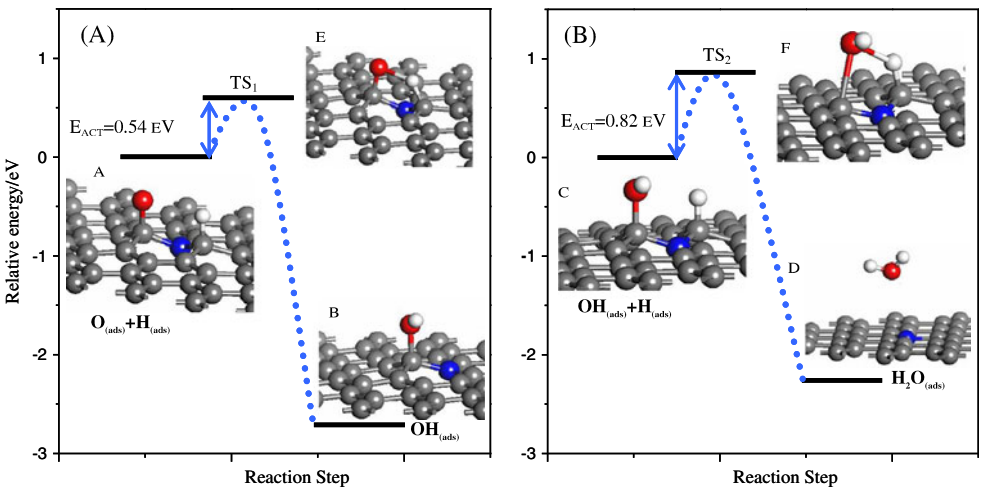

Fig. 5 Relative reaction energy and activation barrier of $O_{(ads)}$ and $OH_{(ads)}$ reduction on the surface together with the optimized reactant and product structures and the corresponding transition structures. **a** Reduction of $O_{(ads)}$ and **b** reduction of $OH_{(ads)}$

dissociation (1.18 eV). Therefore, in terms of thermodynamics and kinetics, $OOH_{(ads)}$ was more likely to break the O–OH bond along the pathway of hydrogenation dissociation. After comparing the three possibilities of $OOH_{(ads)}$ dissociation pathways, we found that the reaction that formed $H_2O_{(ads)}$ and $O_{(ads)}$ possessed the lowest reaction barrier (0.55 eV). Therefore, $O_{(ads)}$ and $H_2O_{(ads)}$ were the favorable reduction products of $OOH_{(ads)}$ dissociation. As shown in Fig. 4b, the generated H_2O molecule drifted away from the surface. Thus, only the isolated $O_{(ads)}$ atom was considered but without the interaction between $O_{(ads)}$ atom and H_2O molecule.

The isolated $O_{(ads)}$ atom preferred to adsorb on the C atom next to the N atom with an adsorption energy of −3.36 eV. We further added a H atom to the system near the O atom. After optimization, the $O_{(ads)}$ atom was reduced by the H atom, and an OH species was formed. The reaction is expressed in Eq. (8). The generated $OH_{(ads)}$ was still chemisorbed on the C atom with an adsorption energy of −1.53 eV. When another H was introduced into the system, the $OH_{(ads)}$ species was reduced, and the second H_2O molecule was formed. The formed H_2O molecule drifted away from the surface, and the distance between the molecule and the surface was 3.12 Å. The reaction is expressed in Eq. (9). Figure 5 shows the optimized structures of the initial, transition, and final states of $O_{(ads)}$ and $OH_{(ads)}$ reduction on GNDG together with the corresponding activation barrier and reaction energy.

$$O_{(ads)} + H^+ + e^- \rightarrow OH_{(ads)} \quad (8)$$

$$OH_{(ads)} + H^+ + e^- \rightarrow H_2O_{(ads)} \quad (9)$$

After comparing the active barriers of all steps, we found that the most favorable four-electron ORR pathway was arranged in the following order: reduction of O_2 into OOH, hydrogenation dissociation of OOH to generate H_2O and O species, reduction of O into OH, and reduction of OH into the second H_2O molecule. The reduction of $OH_{(ads)}$ into H_2O had the highest barrier (0.82 eV). Therefore, the $OH_{(ads)}$ reduction was the rate-determining step in the four-electron reaction, which is similar to the result of ORR on Pt [43, 44, 47], where the rate of $OH_{(ads)}$ removal or protonation determined the overall ORR activity.

Conclusion

This work studied the mechanism of ORR on N-doped graphene. All possible reaction pathways and the transition state of each elementary step were investigated. The results confirmed that the N-doped graphene possessed ORR activity. The C atoms next to the doped N atom were the catalytically active sites. Pathways for both two-electron and four-electron reductions were possible. Both H_2O and H_2O_2 were the products of oxygen reduction. The reduction of OOH into H_2O_2 was easier than O–OH breaking. This reduction followed a direct ER mechanism (the OOH species was in gas phase, but H was chemisorbed on the surface) with a significantly low reaction barrier of 0.09 eV. The rate-determining step for the two-electron pathway was the reduction of O_2 with a reaction barrier of 0.63 eV. However, the rate-determining step for the four-electron pathway was the reduction of OH with a reaction barrier of 0.82 eV. After comparing the barriers of the rate-determining steps of the two pathways with each other, we found that the two-electron pathway was more energetically favored than the four-electron pathway.

Acknowledgments The calculations were performed at the Shanghai Supercomputing Center. This work was supported by the Natural Science Foundation of China (Nos. 20673135 and 50702065), Shanxi Natural Science Foundation (2008021029-1), and Knowledge Innovation Project of Chinese Academy of Science (No. KJCX2.YW.M10).

References

1. Xiong W, Du F, Liu Y, Perez A, Supp M, Ramakrishnan TS, Dai L, Jiang L (2010) J Am Chem Soc 132:15839–15841
2. Chen Z, Higgins D, Tao H, Hsu RS, Chen Z (2009) J Phys Chem C 113:21008–21013
3. Steele BC, Heinzel A (2001) Nature 414:345–352
4. Winter M, Brodd RJ (2004) Chem Rev 104:4245–4270
5. Gasteiger HA, Kocha SS, Sompalli B, Wagner FT (2005) Appl Catal B 56:9–35
6. Yu X, Ye S (2007) J Power Sources 172:145–154
7. Gong KP, Du F, Xia ZH, Durstock M, Dai LM (2009) Science 323: 760–764
8. Qu L, Liu Y, Baek J-BDai L (2010) ACS Nano 4:1321–1326
9. Geng DS, Chen Y, Chen YG, Li YL, Li RY, Sun XL, Ye SY, Knights S (2011) Energy Environ Sci 4:760–764
10. Kundu S, Nagaiah TC, Xia W, Wang YM, Van Dommele S, Bitter JH, Santa M, Grundmeier G, Bron M, Schuhmann W, Muhler M (2009) J Phys Chem C 113:14302–14310
11. Niwa H, Kobayashi M, Horiba K, Harada Y, Oshima M, Terakura K, Ikeda T, Koshigoe Y, Ozaki J-i, Miyata S, Ueda S, Yamashita Y, Yoshikawa H, Kobayashi K (2011) J Power Sources 196:1006–1011
12. Niwa H, Horiba K, Harada Y, Oshima M, Ikeda T, Terakura K, Ozaki J-iMiyata S (2009) J Power Sources 187:93–97
13. Tang YF, Allen BL, Kauffman DR, Star A (2009) J Am Chem Soc 131:13200–13201
14. Wang Y, Shao YY, Matson DW, Li JH, Lin YH (2010) ACS Nano 4: 1790–1798
15. Vanin M, Gath J, Thygesen KS, Jacobsen KW (2010) Phys Rev B 82: 195411 doi: 10.1103/PhysRevB.82.195411
16. Wang Z, Jia R, Zheng J, Zhao J, Li L, Song J, Zhu Z (2011) ACS Nano 5:1677–1684
17. Ma G, Jia R, Zhao J, Wang Z, Song C, Jia S, Zhu Z (2011) J Phys Chem C 115:25148–25154
18. Matter PH, Ozkan US (2006) Catal Lett 109:115–123
19. Maldonado S, Stevenson KJ (2005) J Phys Chem B 109:4707–4716
20. Chen S, Bi J, Zhao Y, Yang L, Zhang C, Ma Y, Wu Q, Wang XHZ (2012) Adv Mater 24:5593–5597
21. Zhang S, Zhang H, Liu Q, Chen S (2013) J Mater Chem A 1: 3302–3308

22. Deng DH, Pan XL, Yu LA, Cui Y, Jiang YP, Qi J, Li WX, Fu QA, Ma XC, Xue QK, Sun GQ, Bao XH (2011) Chem Mater 23:1188–1193
23. Lee KR, Lee KU, Lee JW, Ahn BT, Woo SI (2010) Electrochem Commun 12:1052–1055
24. Huang S-F, Terakura K, Ozaki T, Ikeda T, Boero M, Oshima M, Ozaki J-iMiyata S (2009) Phys Rev B 80:235410
25. Kim H, Lee K, Woo SI, Jung Y (2011) Phys Chem Chem Phys 13: 17505–17510
26. Zhang L, Xia Z (2011) J Phys Chem C 115:11170–11176
27. Ikeda T, Boero M, Huang S-F, Terakura K, Oshima M, Ozaki J-I (2008) J Phys Chem C 112:14706–14709
28. Sidik RA, Anderson AB, Subramanian NP, Kumaraguru SP, Popov BN (2006) J Phys Chem B 110:1787–1793
29. Lai L, Potts JR, Zhan D, Wang L, Poh CK, Tang C, Gong H, Shen Z, Lin J, Ruoff RS (2012) Energy Environ Sci 5:7936–7942
30. Xu Z, Li H, Fu M, Luo H, Sun H, Zhang L, Li K, Wei B, Lu J, Zhao X (2012) J Mater Chem 22:18230–18236
31. Okamoto Y (2009) Appl Surf Sci 256:335–341
32. Luo Z, Lim S, Tian Z, Shang J, Lai L, MacDonald B, Fu C, Shen Z, Yu T, Lin J (2011) J Mater Chem 21:8038–8044
33. Yu L, Pan X, Cao X, Hu P, Bao X (2011) J Catal 282:183–190
34. Payne MC, Teter MP, Allan DC, Arias T, Joannopoulos J (1992) Rev Mod Phys 64:1045–1097
35. Milman V, Winkler B, White J, Pickard C, Payne M, Akhmatskaya E, Nobes R (2000) Int J Quantum Chem 77:895–910
36. Perdew JP, Burke K, Ernzerhof M (1996) Phys Rev Lett 77:3865
37. Perdew JP, Chevary J, Vosko S, Jackson KA, Pederson MR, Singh D, Fiolhais C (1992) Phys Rev B 46:6671
38. Ge Q, Jenkins S, King D (2000) Chem Phys Lett 327:125–130
39. Dai JY, Yuan JM (2010) Phys Rev B 81:165414
40. Zhao L, He R, Rim KT, Schiros T, Kim KS, Zhou H, Gutiérrez C, Chockalingam S, Arguello CJ, Pálová L (2011) Science 333: 999–1003
41. Wang Y, Balbuena PB (2005) J Phys Chem B 109:14896–14907
42. Rossmeisl J, Qu Z-W, Zhu H, Kroes G-JNørskov JK (2007) J Electroanal Chem 607:83–89
43. Hyman MP, Medlin JW (2006) J Phys Chem B 110:15338–15344
44. Zhang J, Vukmirovic MB, Xu Y, Mavrikakis M, Adzic RR (2005) Angew Chem Int Ed 44:2132–2135
45. Damjanovic A, Brusic V (1967) Electrochim Acta 12:615–628
46. Jacob T, Goddard WA (2006) Chem Phys Chem 7:992–1005
47. Nilekar AU, Mavrikakis M (2008) Surf Sci 602:L89–L94
48. Tripković V, Skúlason E, Siahrostami S, Nørskov JK, Rossmeisl J (2010) Electrochim Acta 55:7975–7981
49. Wang J, Markovic N, Adzic R (2004) J Phys Chem B 108: 4127–4133
50. Studt F (2013) Catal Lett 143:58–60
51. Eley D, Rideal E (1940) Nature 146:401–402
52. Kuipers E, Vardi A, Danon A, Amirav A (1991) Phys Rev Lett 66:116
53. Meijer AJHM, Farebrother AJ, Clary DC, Fisher AJ (2001) J Phys Chem A 105:2173–2182